Shaolin Yang,[1,2,3] Minjie Wu,[1] Olusola Ajilore,[1] Melissa Lamar,[1] and Anand Kumar[1]

Metabolic Aberrations Impact Biophysical Integrity of Macromolecular Protein Pools in the Default Mode Network

Diabetes 2016;65:3464–3472 | DOI: 10.2337/db15-1714

PATHOPHYSIOLOGY

The brain's default mode network (DMN), having a high rate of basal energy metabolism, is vulnerable to altered glucose metabolism in type 2 diabetes mellitus (T2DM) due to insulin resistance and chronic hyperglycemia. Previous studies showed that functional connectivity and structural connectivity among the DMN nodal regions are compromised in T2DM. We applied magnetization transfer imaging to examine the impact of T2DM on the biophysical integrity of the DMN. The results showed that the biophysical integrity of macromolecular protein pools in the posterior cingulate cortex (PCC), a central DMN hub region, was selectively compromised in T2DM, whereas the other nodal regions of the DMN, including the medial prefrontal cortex, lateral inferior parietal cortex, precuneus, and medial and lateral temporal cortices, were biophysically intact compared with those of control subjects without diabetes. Furthermore, the degree of biophysical impairment of the PCC correlated with both hyperglycemia and vascular compromise, the two physiological hallmarks of diabetes. These new findings demonstrate that the PCC is vulnerable in the DMN and may shed light on the molecular neurobiology of T2DM and help to elucidate the pathophysiology of diabetes-related cognitive comorbidities and increased risk for dementia.

Type 2 diabetes mellitus (T2DM), associated with metabolic and vascular complications, often is accompanied by brain changes and behavioral aberrations, including mood disorders, cognitive impairment, and increased risk of developing dementia, especially Alzheimer disease (AD) (1,2). T2DM, therefore, is an ideal model for studying the impact of metabolic and vascular changes on the brain, particularly the brain regions and networks with a high level of basal glucose metabolism, such as the default mode network (DMN) (3–6).

The brain's DMN is a neural network that is most active at rest but "deactivated" when the brain is focused on external, goal-directed, attentionally demanding tasks (6). It comprises a core set of brain regions that show strong intrinsic functional correlation, including the areas in the posterior cingulate cortex (PCC), precuneus (PCu), medial prefrontal cortex (mPFC), and lateral inferior parietal cortex (3,4,6). Depending on the analytic approach, the network can also include other, less prominent regions in the DMN map, such as the areas in the medial and lateral temporal cortices (3,7,8). Activity within this network is considered to be an intrinsic aspect of brain functioning and has been posited to be a component of consciousness, sense of self, self-referential processing, and episodic memory (3,6,9). Besides possessing an inherently high level of basal glucose metabolism, the DMN has the highest rate of aerobic glycolysis (a form of glucose metabolism outside oxidative phosphorylation) than any other neural networks in the brain as measured by fluorine-18 fluorodeoxyglucose positron emission tomography (6,10–12). This highly metabolically active property sets the DMN apart from other neural networks (6) and renders it preferentially vulnerable to altered glucose metabolism in T2DM as the result of chronic hyperglycemia and insulin resistance. Compared with healthy control subjects (HCs), patients with T2DM show compromised functional connectivity and structural connectivity (i.e., white matter [WM] fibers)

[1]Department of Psychiatry, University of Illinois at Chicago, Chicago, IL
[2]Department of Radiology, University of Illinois at Chicago, Chicago, IL
[3]Department of Bioengineering, University of Illinois at Chicago, Chicago, IL

Corresponding author: Shaolin Yang, syang@psych.uic.edu, and Anand Kumar, akumar@psych.uic.edu.

Received 17 December 2015 and accepted 29 July 2016.

This article contains Supplementary Data online at http://diabetes.diabetesjournals.org/lookup/suppl/doi:10.2337/db15-1714/-/DC1.

among the DMN nodal regions (13,14). However, no studies to date have examined the biophysical integrity of the nodal regions of the DMN. Maintaining the biophysical integrity of brain tissue is critical to normal brain function but highly relies on energy supply from glucose metabolism; thus, it is sensitive to metabolic aberrations, such as in T2DM. In this study, an alternative, biophysical view of the impact of T2DM on the brain's DMN is established. This information may improve our understanding of the mechanisms underlying T2DM-related brain alterations and the neurobiology of diabetes and its heightened risk for other neurological and psychiatric diseases, such as AD and depression.

We applied magnetization transfer (MT) imaging to examine the biophysical integrity of macromolecular protein pools in the nodal regions of the DMN in patients with T2DM and HCs. The primary outcome measure of MT imaging is the magnetization transfer ratio (MTR), which reflects the biophysical integrity of macromolecular protein compartments and their local microenvironments (15). Postmortem MT and histopathology studies revealed that lower MTR in WM is correlated with myelin compromise and/or axonal loss (16,17). In gray matter (GM), reduced MTR is a biophysical measurement that reflects aberrations in cell membrane proteins and phospholipids (18,19). Injury to cell membranes and reductions in dendritic density as well as neuronal size and number may alone or in combination be responsible for reduced MTR in GM (20).

To the best of our knowledge, this is the first MT study to examine the biophysical integrity of macromolecular protein pools in the DMN of patients with T2DM. We hypothesized that MTR would be lower in the DMN nodal regions of patients with T2DM than in HCs. We also hypothesized that MTR in the DMN nodal regions would be negatively correlated with clinical measures that reflect cerebrovascular comorbidities and blood glucose regulation. Examination of the biophysical integrity of macromolecular protein pools in the DMN of patients with T2DM may shed light on the molecular neurobiology of diabetes and help to clarify the pathophysiology of diabetes-related neuropsychological and cognitive comorbidities.

RESEARCH DESIGN AND METHODS

Subjects

The study population comprised 21 patients with T2DM but without mood disorders and 27 HCs without diabetes (Table 1). The subjects were selected from a larger sample recruited to a research program that investigated diabetes and depression at the University of Illinois at Chicago. All participants were age ≥30 years and recruited from the greater Chicago area through flyers, local advertisements, and relevant outpatient clinics. The study was approved by the University of Illinois at Chicago institutional review board, and written informed consent was obtained from all subjects.

The diagnosis of T2DM was made by patients' primary care physicians and confirmed using the American Diabetes Association guidelines (an elevated nonfasting hemoglobin A_{1c} [HbA_{1c}] level >6.5% [48 mmol/mol]) (21) or the use of antidiabetic medications (oral hypoglycemic medicine and/or insulin) on enrollment. The subjects with T2DM reported using oral hypoglycemic medications and/or insulin for glycemic control (seven with one oral hypoglycemic medication or insulin, seven with two or more hypoglycemic medications, two with both medications and insulin, and five without hypoglycemic medication or insulin). With respect to diabetic vascular complications (22), 4 subjects had diabetic microvascular complications (3 diabetic neuropathy, 1 retinopathy), 3 had diabetic macrovascular complications (2 coronary artery disease, 1 both peripheral arterial disease and coronary artery disease), 1 had both, and 13 had no vascular complications. HCs were free of diabetes and had HbA_{1c} levels within the normal limits. All subjects underwent evaluation with the Mini-Mental State Examination (MMSE) (23), a Structured Clinical Interview for DSM-IV (24), and the 17-item Hamilton Depression Rating Scale (HDRS) (25), which were administered by a trained research assistant and a board certified (A.K.) or board eligible (O.A.) psychiatrist. All subjects denied a history of depressed mood, obtained scores of ≤8 on the HDRS, and were free of unstable medical conditions.

Exclusion criteria were any current or history of neurological and psychiatric disorders (e.g., dementia, stroke, seizure, transient ischemic attack, and depression), learning disability or attention deficit hyperactivity disorder, psychotropic medication use, current or history of substance abuse or dependence (except for tobacco smoking), history of head injury or loss of consciousness, an MMSE score <26, or any contraindication to MRI scanning, such as metal in the body, surgically implanted devices containing metal, claustrophobia, and pregnancy.

All subjects were assessed for medical comorbidities with the Cumulative Illness Rating Scale (CIRS) (26) and for vascular comorbidities with the Framingham Stroke Risk Profile (FSRP) score (27). We also designed a modified FSRP (mFSRP) score in which the contribution of T2DM was removed, thereby representing vascular compromise only. All subjects were also administered the Center for Epidemiologic Studies of Depression (CESD) scale (28) as an independent measure of depression severity. All subjects received a nonfasting blood draw to document the HbA_{1c} level, an indicator of glycemic control, and HDL and LDL cholesterol levels. Systolic blood pressure (SBP) and diastolic blood pressure (DBP) and BMI were documented. In addition, the Wechsler Test of Adult Reading (WTAR) (29) was used to assess subjects' IQ.

MT Imaging and MRI Data Acquisition

MT imaging exploits magnetization exchange between protons bound to macromolecules and free protons in tissue water (Fig. 1). In the brain, bound protons are primarily present in myelin in WM and in cell membrane proteins and phospholipids in GM. Compared with free protons, bound protons are less mobile and possess a very

Table 1—Demographic and clinical measures between subject groups

			Statistics		
	HC (n = 27)	T2DM (n = 21)	F	df	P value
Age (years)	63.15 ± 12.76	64.81 ± 11.70	0.215	1,46	0.645
Sex			χ^2 = 0.762	1	0.383
Male	12	12			
Female	15	9			
Race			χ^2 = 3.892	4	0.421
Black	10	11			
Hispanic	2	1			
Asian	2	0			
White	11	9			
Other	2	0			
Handedness			χ^2 = 2.938	2	0.230
Right	25	16			
Left	2	4			
Mixed	0	1			
Education (years)	14.56 ± 1.95	14.86 ± 2.24	0.249	1,46	0.620
WTAR IQ	101.68 ± 11.63	98.95 ± 16.30	0.437	1,44[a]	0.512
MMSE	28.85 ± 1.03	28.24 ± 1.26	3.457	1,46	0.069
HDRS	0.85 ± 1.10	1.76 ± 1.87	4.446	1,46	**0.040**
CESD	5.59 ± 4.81	7.19 ± 5.38	1.176	1,46	0.284
BMI (kg/m^2)	29.83 ± 17.23	32.10 ± 6.53	0.326	1,46	0.571
SBP (mmHg)	137.96 ± 14.06	139.62 ± 17.48	0.133	1,46	0.718
DBP (mmHg)	80.26 ± 9.96	83.71 ± 10.04	1.411	1,46	0.241
T2DM duration (months)	—	113.10 ± 83.56	—	—	—
LDL cholesterol	97.52 ± 27.72	89.10 ± 22.55	1.279	1,46	0.264
HDL cholesterol	72.74 ± 22.30	48.00 ± 12.95	20.434	1,46	**<0.001**
CIRS	3.56 ± 2.86	7.24 ± 3.00	18.775	1,46	**<0.001**
FSRP	9.00 ± 4.71	13.00 ± 4.78	8.424	1,46	**0.006**
mFSRP	9.00 ± 4.71	10.57 ± 5.02	1.243	1.46	0.271
HbA_{1c}			24.711	1,46	**<0.001**
%	5.67 ± 0.35	7.30 ± 1.66			
mmol/mol	38 ± 3.8	56 ± 18.1			

Data are mean ± SD unless otherwise indicated. Boldface indicates significance at $P < 0.05$. [a]Two HCs' WTAR IQ scores were not recorded.

short T_2 relaxation time. As a result, the MR signal from bound protons decays rapidly to noise levels before data acquisition and is therefore undetectable by regular MRI. To solve this problem, an off-resonance prepulse is applied in MT to selectively presaturate bound protons. Magnetization is then transferred from saturated bound protons to free protons through chemical exchange or direct dipolar coupling. This transfer of magnetization leads to a reduced MR signal of free protons (Fig. 1). The contrast between images with and without the off-resonance saturation prepulse, defined as MTR, indirectly measures bound protons and, accordingly, informs the biophysical integrity of macromolecular protein pools and their local microenvironments in brain tissue (15). As demonstrated in postmortem brain MT studies (16,17), lower MTR in WM is associated with demyelination and lower axonal density. The origins of MTR changes in GM are more complex and heterogeneous and may reflect multiple neurobiological aberrations (17–20). The biophysical correlates of lower MTR in GM are believed to be linked to impaired cell membrane proteins and phospholipids besides neuronal and synaptic loss (20,30–32). Wallerian degeneration, which is secondary to proximal and/or distal axonal damage, also has been implicated as a mechanism contributing to lower MTR (18,20). However, the exact biochemical and biophysical underpinnings of MTR in vivo are not well understood. MTR can be altered by other diseases, such as multiple sclerosis (33) and schizophrenia (34). Additionally, lower MTR is found in WM lesions (WM loss or leukoaraiosis) (35). The alterations in MTR in vivo may be due to various mechanisms. Although lacking specificity in its origins, MT imaging provides an innovative way to probe the integrity of macromolecular proteins and phospholipids in the brain.

The MRI scans were performed on a Philips Achieva 3.0T X-Series MRI scanner (Philips Medical Systems, Best,

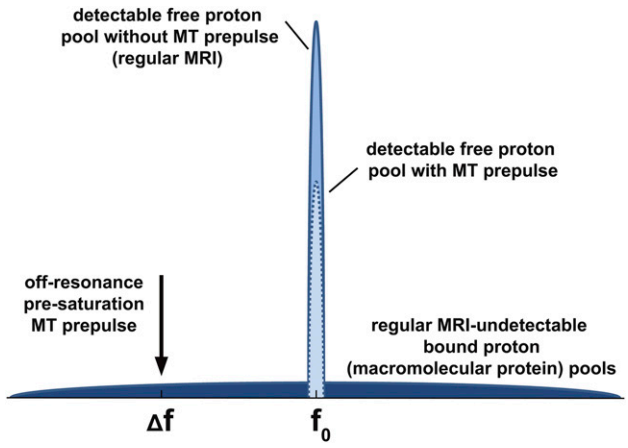

Figure 1—Schematic diagram of the basic principles of MT imaging.

the Netherlands) with an eight-channel sensitivity encoding head coil. Subjects were equipped with soft ear plugs, positioned comfortably in the head coil by using custom-made foam pads to minimize head motion, and instructed to remain still. The MT images were acquired using a three-dimensional spoiled gradient-echo sequence with multishot echo-planar imaging readout and the following parameters: repetition time (TR) 64 ms, echo time (TE) 15 ms, flip angle 9°, field of view (FOV) 24 cm, 67 axial slices, slice thickness 2.2 mm without gap, echo-planar imaging factor 7, reconstructed voxel size 0.83 × 0.83 × 2.2 mm^3, with a nonselective five-lobed Sinc-Gauss off-resonance MT prepulse (B_1 10.5 μT, Δf 1.5 kHz, duration 24.5 ms) optimized for maximum WM/GM contrast (36). The image slices were parallel to the anterior commissure–posterior commissure line. Parallel imaging was used with a reduction factor of 2. Before the MT scan, high-resolution three-dimensional T_1-weighted magnetization-prepared rapid acquisition gradient echo (MPRAGE) images were acquired for registration between different image modalities in postprocessing. The MPRAGE sequence parameters were TR 8.4 ms, TE 3.9 ms, flip angle 8°, FOV 24 cm, 134 axial slices without gap, and reconstructed voxel size 0.83 × 0.83 × 1.1 mm^3. In addition, T_2-weighted fluid-attenuated inversion recovery images were acquired using turbo spin echo sequence with the following sequence parameters: TR 11,000 ms, inversion time 2,800 ms, TE 68 ms, FOV 24 cm, 67 axial slices without gap, and reconstructed voxel size 0.83 × 0.83 × 2.2 mm^3 for delineation of hyperintense areas in the brain.

Image Processing

The images with (M_s) and without the off-resonance (M_0) MT prepulse in the MT scan were coregistered first. The MTR values were calculated from the coregistered M_0 and M_s on a voxel-by-voxel basis using the equation MTR = $(M_0 - M_s)/M_0$. The M_s image was further registered with the T_1-weighted MPRAGE image for intrasubject alignment. Skull stripping was performed on both images (M_s and T_1-weighted images) before the coregistration for improved accuracy. By using FreeSurfer software (https://surfer.nmr.mgh.harvard.edu), the cortical surface of individual T_1-weighted images was vertexwise mapped to a common surface based on cortical folding patterns (individual T_1-weighted surface → fsaverage surface). Furthermore, by using the combined volume and surface-based registration method, individual T_1-weighted image was voxelwise mapped to the standard MNI152 image space (individual T_1-weighted volume → MNI152 volume).

The DMN map can be obtained using resting-state functional MRI with high reliability and replicability. In this study, the well-validated and replicated DMN map (MNI152 standard space) was obtained from the seminal study of Smith et al. (37) and converted to a binary DMN mask (threshold $P < 0.0001$), which was used to derive the DMN regions in individual MT space. The obtained DMN mask (Fig. 2) encompasses the medial parietal

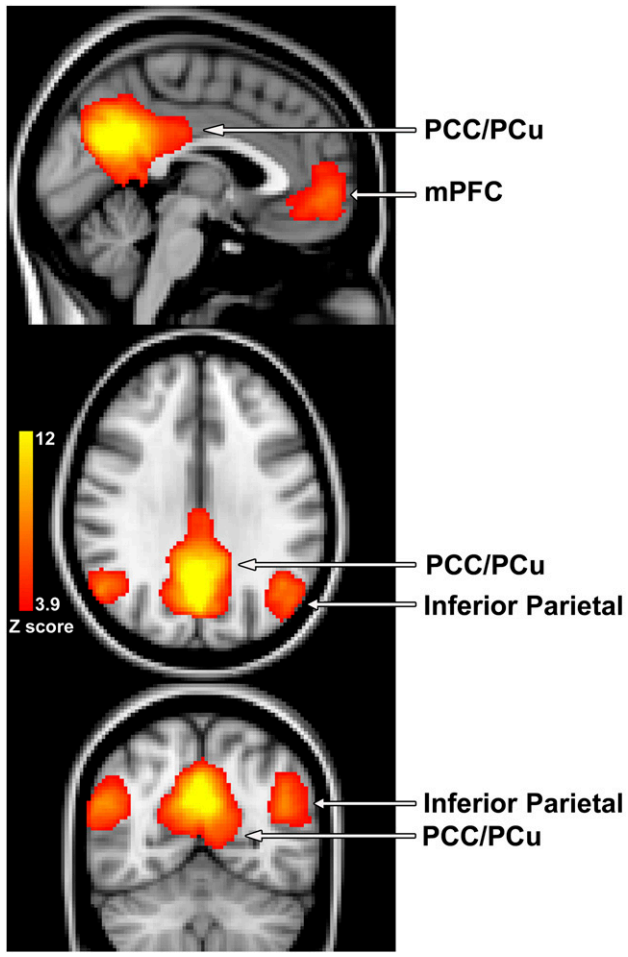

Figure 2—Mask ($P < 0.0001$) of the core set of brain regions of the DMN, obtained by independent component analysis of resting state functional MRI data of healthy adult subjects from a third party (37).

(including PCC/PCu), bilateral inferior parietal, and mPFC regions. With the computed individual T_1-weighted surface → fsaverage surface mapping and T_1-weighted → MNI152 volumetric transformation along with the T_1-weighted and MT coregistration, the DMN mask was mapped into individual T_1-weighted surface/volume space and was further parcellated into DMN regions in the individual MT space. Additionally, anatomical masks of PCC and PCu were applied to the DMN mask to obtain individual PCC and PCu divisions of the medial parietal part of the DMN (Supplementary Fig. 1).

Average MTR values were calculated in each of the core DMN regions, i.e., PCC, PCu, mPFC, and inferior parietal regions in the left and right hemispheres. We examined the MTR in the GM and superficial WM of the DMN nodal regions. Superficial WM lies immediately beneath GM, consists of short association fibers, and connects neighboring gyri within the DMN nodal regions. The superficial WM component of the DMN nodal regions was evaluated by the MTR values of the superficial WM sampled along the WM surface normal from 1 to up to 5 mm of the distance to the WM surface. In this way, we evaluated the superficial WM immediately beneath the GM component of the DMN nodal regions rather than the artifactual spreading into the WM from the blood oxygen level–dependent signal in the GM or as a result of the smoothing procedure during preprocessing.

In the literature, the DMN often also includes the hippocampus and surrounding areas (e.g., parahippocampus) in the medial temporal lobe and areas in the lateral temporal cortex, which are less prominent in the DMN maps than the core set of DMN regions (3). Consistent with the literature, there were no areas in the medial and lateral temporal cortices in the DMN mask ($P < 0.0001$) as used to define the clusters of the core DMN nodal regions. To define DMN regions of interest in the medial and lateral temporal lobes, we reduced the threshold to $P < 0.05$ and calculated the MTR in the DMN clusters of these two regions. For exploratory purposes, we also calculated the MTR in the core set of DMN regions within the DMN mask at the reduced threshold $P < 0.05$ (Supplementary Fig. 2).

Statistical Analysis

Clinical and demographic measures were analyzed using univariate ANOVA for continuous variables and χ^2 tests for categorical variables. Group differences in MTR in bilateral DMN regions were assessed using mixed-model analysis with diagnostic group as the between-group factor and hemisphere and tissue type (GM or WM) as the within-subject factors. Correlations between MTR and FSRP score, HbA_{1c} level, or other T2DM-related clinical measures were analyzed using partial Pearson product moment correlations, controlling for age and/or other covariates. In the correlation analysis of MTR and HbA_{1c}, a natural logarithm transformation was first performed on HbA_{1c} (i.e., log-transformed HbA_{1c}) to minimize the skewness of this variable in the combined sample from the HC and T2DM groups. Correction for multiple comparisons was performed by using the false discovery rate approach (38–40), with the maximum acceptable false discovery rate threshold set at 0.1. All statistical analyses were carried out with SPSS version 22 software (IBM Corporation, Chicago, IL).

RESULTS

Demographic and Clinical Characteristics of the T2DM and HC Groups

Table 1 summarizes the demographic and clinical characteristics of the T2DM and HC groups. There were no significant group differences in age, sex, race, handedness, education, WTAR IQ, MMSE, CESD, BMI, SBP, DBP, LDL cholesterol, and mFSRP. Although there was a group difference in HDRS, both groups were free of depression, with very-low mean scores (<2). As expected, there were significant group differences in diabetes-related clinical measures (HDL cholesterol: $F = 20.434$ [$df = 1,46$], $P < 0.001$; CIRS: $F = 18.775$ [$df = 1,46$], $P < 0.001$; FSRP: $F = 8.424$ [$df = 1,46$], $P = 0.006$; HbA_{1c}: $F = 24.711$ [$df = 1,46$], $P < 0.001$).

Obesity, hypertension, vascular disease, and/or elevated LDL cholesterol level often are seen in patients with T2DM. Each comorbidity has been reported to exert its own effects on the brain. In this study, these comorbidities, represented by BMI, SBP, DBP, mFSRP, and LDL, were of comparable levels between the two subject groups ($P > 0.24$), so the possible effects of these comorbidities on the group difference in MTR have been minimized and the findings are primarily attributable to T2DM.

Group Differences in Biophysical Integrity of DMN Regions Measured by MTR

By using the mixed-model analysis, we analyzed the MTR measures of both GM and WM in the nodal regions of the DMN, with diagnostic group as the between-group factor and hemisphere and tissue type (GM or WM) as the within-subject factors. We found that the MTR of PCC was significantly lower in patients with T2DM than in HCs ($F = 5.853$ [$df = 1,46$], $P = 0.020$), which survived the multiple comparisons correction. In contrast, there were no significant group differences in the other core DMN regions (inferior parietal: $F = 1.352$ [$df = 1,46$], $P = 0.251$; mPFC: $F = 0.229$ [$df = 1,46$], $P = 0.634$; PCu: $F = 1.150$ [$df = 1,46$], $P = 0.289$). Post hoc analyses revealed that compared with HCs, patients with T2DM exhibited significantly lower MTR in PCC WM ($F = 7.443$ [$df = 1,46$], $P = 0.009$) (Fig. 3*A*) and PCC GM ($F = 4.069$ [$df = 1,46$], $P = 0.050$) (Fig. 3*B*). The reduced level of significance in the PCC GM may be due to larger partial volume effects (from the cerebrospinal fluid) of the MTR measurement in the GM than that in the WM.

Because no areas in the medial and lateral temporal regions survived in the DMN mask at $P < 0.0001$ (Fig. 2), a second DMN mask was generated at a reduced threshold of $P < 0.05$ to define the DMN areas in the medial and lateral temporal cortices (RESEARCH DESIGN AND METHODS).

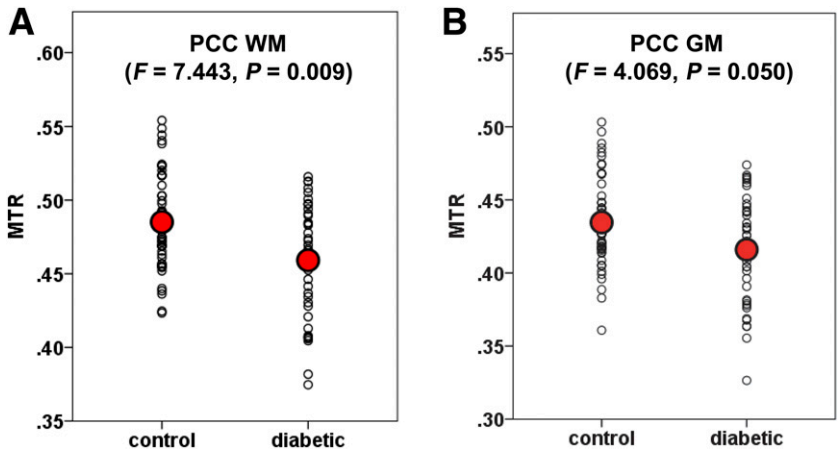

Figure 3—Biophysical integrity of macromolecular protein pools as measured by MTR in the PCC within the DMN mask ($P < 0.0001$) in 21 patients with T2DM and 27 matched HCs. *A*: Mixed-model analysis (with diagnostic group as the between-group factor and hemisphere as a within-subject factor) of MTR in the WM portion of the PCC within the DMN mask ($F = 7.443$ [$df = 1,46$], $P = 0.009$). *B*: Mixed-model analysis of MTR in the GM portion of the PCC within the DMN mask ($F = 4.069$ [$df = 1,46$], $P = 0.050$). Individual data points are shown; red points represent group means.

We found no group differences in MTR in the DMN areas in either the medial temporal cortex ($F = 0.320$ [$df = 1,46$], $P = 0.574$) or the lateral temporal cortex ($F = 0.293$ [$df = 1,46$], $P = 0.591$). In contrast, with the DMN mask at a reduced threshold of $P < 0.05$, the significant group difference of MTR in the PCC still held ($F = 6.846$ [$df = 1,46$], $P = 0.012$) (post hoc analysis results presented in Supplementary Fig. 2) and survived the multiple comparisons correction, whereas no group differences were found in the other core regions of the DMN ($P > 0.32$).

Correlation Between Biophysical Integrity of PCC and Clinical Measures

Hyperglycemia and vascular compromise are two biological hallmarks of T2DM. We found that in the combined group, MTR negatively correlated with the log-transformed HbA_{1c} level in the left-side PCC WM ($r = -0.310$ [$df = 45$], $P = 0.034$) (Fig. 4*A*) and approached significance in the right-side PCC WM ($r = -0.248$ [$df = 45$], $P = 0.093$) (Fig. 4*B*). Additionally, MTR in bilateral PCC WM was negatively correlated with the FSRP score across the entire sample (left-side PCC: $r = -0.367$ [$df = 45$], $P = 0.011$; right-side PCC: $r = -0.383$ [$df = 45$], $P = 0.008$) (Fig. 5*A* and *B*). We found a trend to significance in the correlation between MTR in the PCC GM and the FSRP score ($P > 0.07$). In contrast, there were no significant associations between MTR and SBP, DBP, BMI, CIRS, and CESD ($P > 0.12$). Although correlations do not prove causality, these correlations suggest that both hyperglycemia and cerebrovascular compromise contribute to the biophysical impairments of macromolecular proteins pools in the PCC.

Group Differences in Other Related MRI Measures

T2DM reportedly is linked to leukoaraiosis or WM hyperintensities (41,42) and brain atrophy (42), which are particularly relevant in this study because MTR may be altered in the presence of these conditions. Therefore, we evaluated the possible differences in WM hyperintensities (43) and brain atrophy between the HC and T2DM groups and found no significant group differences in WM hyperintensities ($P > 0.18$) and regional cortical atrophy ($P > 0.26$).

DISCUSSION

The main finding of this study is that the biophysical integrity of macromolecular protein pools in the PCC, the central hub region of the brain's DMN, is compromised in patients with T2DM compared with HCs, whereas no significant group differences were found in the biophysical integrity of macromolecular protein pools in the other nodal regions of the DMN. Furthermore, the biophysical integrity of macromolecular protein pools in the PCC, as assessed by MTR, are negatively correlated with two key T2DM-related clinical measures: HbA_{1c} level, which reflects glycemic control, and vascular risk factors as assessed by FSRP score.

The PCC, which consists of Brodmann areas 23 and 31, has dense structural connectivity to widespread regions of the brain and is involved in heterogeneous functions, including default mode–related, internally directed thoughts (e.g., autobiographic memory recollection) and active control of cognition and behaviors by integrating information through the hub and regulating the balance between internally and externally directed brain activity (44). Other studies revealed that the PCC itself consists of functionally distinct, but spatially partially overlapping subdivisions, which is in line with its complex, highly heterogeneous functional organization and constant interaction with various neural networks, including executive, attentional, language, and default mode–related networks (44). For example, during an attentionally demanding task, the ventral division of the PCC displays "deactivation" typically associated with the DMN, whereas the dorsal division of the PCC is continuously active, controlling the focus of attention and keeping the brain in a vigilant attention state (45,46). The observed high metabolic rate of oxygen and

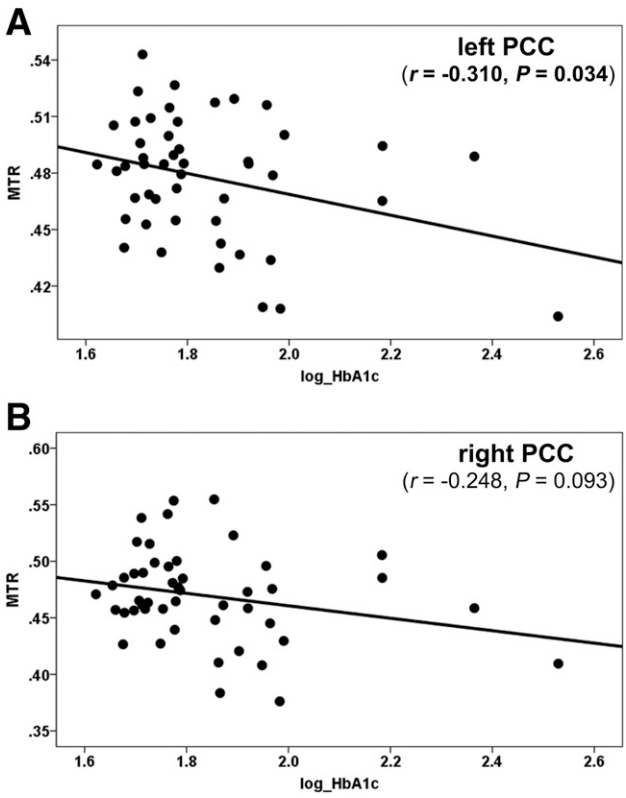

Figure 4—Associations between the biophysical integrity of macromolecular protein pools measured by MTR in the PCC and diabetes-related clinical measure HbA_{1c} level (log-transformed) in the combined groups. Negative correlation between MTR across groups and log-transformed HbA_{1c} level in the left-side PCC WM ($r = -0.310$ [$df = 45$], $P = 0.034$) (*A*) and the right-side PCC WM ($r = -0.248$ [$df = 45$], $P = 0.093$) (*B*).

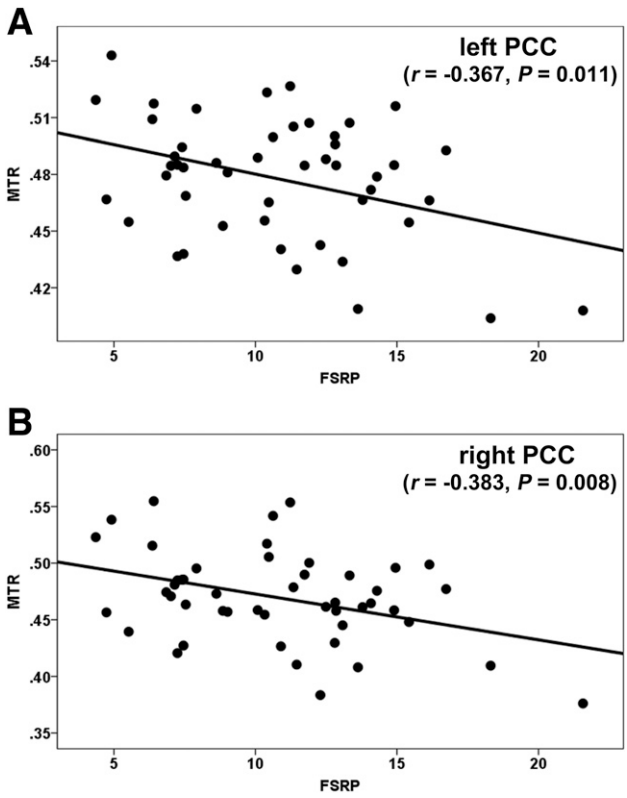

Figure 5—Associations between the biophysical integrity of macromolecular protein pools measured by MTR in the PCC and diabetes-related clinical measure vascular risk factor assessed by FSRP score in the combined groups. Negative correlation between MTR across groups and vascular risk factor assessed by FSRP score in the left-side PCC WM ($r = -0.367$ [$df = 45$], $P = 0.011$) (*A*) and the right-side PCC WM ($r = -0.383$ [$df = 45$], $P = 0.008$) (*B*).

glucose in the PCC (6,10) are consistent with this continuous activity and may partly explain the persistently high level of blood flow and volume within the PCC, as measured by perfusion MRI, during a task or at rest (9).

PCC plus PCu, referred to as "PCC/PCu" in the literature, often are treated as an integrated hub region of the DMN (3,47,48). However, some have suspected that the PCu (consisting of Brodmann area 7m) is not a core component of the DMN (3), whereas others emphasize that the PCu should be a distinct functional core of the DMN (48). Because of these contradictory arguments, we separated PCC and PCu by applying the anatomic masks of PCC and PCu to the DMN mask (RESEARCH DESIGN AND METHODS). The PCC possesses extremely high baseline metabolism, which readily distinguishes itself from PCu. More specifically, the regional cerebral blood flow (rCBF) and cerebral metabolic rate for glucose (CMRglc) in the PCC are ~40% higher than in the combined PCC/PCu area of the DMN (6,47), indicating a significantly higher rate of baseline metabolism in the PCC than in the PCu. Furthermore, although the metabolism in the PCC changes with cognitive state, the fluctuations of rCBF or CMRglc induced by the change of cognitive state are only ~6% of the baseline levels (6,9,47). Therefore, compared with the PCu, the PCC maintains exceptionally high levels of metabolism both at baseline and during active cognitive states. In line with the difference in the level of glucose metabolism, we observed significantly reduced MTR in the PCC (Fig. 3) but not in the PCu in patients with T2DM compared with HCs. The exceptionally high level of metabolism reflected by CMRglc and rCBF and continuously changing activity in the PCC possibly render this region preferentially vulnerable to the metabolic aberrations of T2DM.

In T2DM, functional connectivity, commonly measured as the synchrony of spontaneous blood oxygen level–dependent signal fluctuations, is compromised between the PCC and other nodal regions of the DMN (14). A more recent report indicated that the compromise in functional connectivity within the DMN was probably due to impaired WM tracts connecting the DMN nodal regions (13). The current findings suggest that in addition to impaired structural connectivity within the DMN (13), the biophysical integrity of macromolecular protein pools in the PCC also is compromised in T2DM, which may independently or synergistically contribute to the compromised functional connectivity within the DMN (14). Because energy support from glucose metabolism is required

to maintain the biophysical integrity of brain tissue, including cell membrane turnover in GM and preservation of myelin integrity in WM, the compromised biophysical integrity of macromolecular protein pools in the PCC may be due to altered glucose metabolism in T2DM, including prediabetes and early stages of disease (1).

Although correlations do not prove causality, those observed between lower MTR in the PCC and higher HbA_{1c} levels and increased vascular risk factors suggest that both hyperglycemia and vascular compromise, the two biological hallmarks of T2DM, contribute to the abnormalities of the PCC. In contrast, no significant associations were found between MTR and blood pressure, BMI, CIRS, and CESD in the current sample, suggesting that the impairment of biophysical integrity of macromolecular protein pools in the PCC was more related to T2DM than the comorbidities of the disease.

Individuals with T2DM are at higher risk of the later development of AD or other dementias (2). The mechanism underlying the connection between T2DM and AD, however, is not completely understood. Patients in the preclinical or early stage of AD show a characteristic reduction (~20%) of CMRglc and rCBF in the PCC (12,49). The reduction can begin many years before clinical manifestations (50), suggesting that hypometabolism of the PCC in the DMN is an early biomarker of pathology (12). On the other hand, the findings from the current study indicate that the biophysical integrity of macromolecular protein pools in the PCC of the DMN is impaired in patients with T2DM. This similarity in vulnerability of the PCC in patients with T2DM and with AD may suggest a critical link between the two conditions. That biophysical impairment of macromolecular protein pools in the PCC may be the result of a metabolism-dependent mechanism in the development of AD is intriguing.

Several limitations of this study should be considered. First, the study had a modest sample size, which may not have sufficient power to detect subtle, if any, changes in the biophysical integrity of macromolecular protein pools in the other nodal regions of the DMN besides the PCC. Second, although we recruited subjects from age ≥30 years, the age range of our subject sample was 34–82 years, with a mean age of 63.8 years and a median age of 67 years; therefore, the findings may apply more to middle-aged and older individuals. Third, several subjects with diabetes had different micro- and macrovascular complications, which might have had a potential impact on the results, although no significant group difference in vascular compromise was measured by the mFSRP. Finally, the T2DM group was taking a range of medications for glycemic control. Because these medications were associated with the status or level of hyperglycemia, the main outcome, MTR, might have been influenced.

In conclusion, using MT imaging, we provide a new biological window into the impact of metabolic aberrations in T2DM on the brain's DMN. We report that among the nodal regions of the DMN, the biophysical integrity of macromolecular protein pools in the PCC, a central hub node of the DMN, is compromised in T2DM and that the degree of biophysical impairment of the PCC correlates with both hyperglycemia and vascular compromise. The broad implications of the findings will help us to better conceptualize the relationship between the metabolic abnormalities observed in diabetes and behavioral aberrations, such as mood disorders, cognitive impairment, and increased risk for dementia.

Acknowledgments. The authors thank Peter van Zijl and Joseph S. Gillen (Johns Hopkins University) for the MT sequence.

Funding. This work was supported by National Institute of Mental Health grants R01-MH-63764 and R01-MH-73989. The MT sequence was developed with support of National Institute of Biomedical Imaging and Bioengineering grant P41-EB-015909.

Duality of Interest. No potential conflicts of interest relevant to this article were reported.

Author Contributions. S.Y. contributed to the investigations, imaging protocol design, data acquisition and analysis, and writing of the manuscript. M.W. contributed to the data analysis and writing of the manuscript. O.A. and M.L. contributed to the review of the manuscript. A.K. contributed to the study design and writing of the manuscript. S.Y. and A.K. are the guarantors of this work and, as such, had full access to all the data in the study and take responsibility for the integrity of the data and the accuracy of the data analysis.

Prior Presentation. Parts of this study were presented in abstract form at the 54th Annual Meeting of the American College of Neuropsychopharmacology, Hollywood, FL, 6–10 December 2015.

References

1. Baker LD, Cross DJ, Minoshima S, Belongia D, Watson GS, Craft S. Insulin resistance and Alzheimer-like reductions in regional cerebral glucose metabolism for cognitively normal adults with prediabetes or early type 2 diabetes. Arch Neurol 2011;68:51–57

2. Biessels GJ, Staekenborg S, Brunner E, Brayne C, Scheltens P. Risk of dementia in diabetes mellitus: a systematic review. Lancet Neurol 2006;5:64–74

3. Buckner RL, Andrews-Hanna JR, Schacter DL. The brain's default network: anatomy, function, and relevance to disease. Ann N Y Acad Sci 2008;1124:1–38

4. Greicius MD, Krasnow B, Reiss AL, Menon V. Functional connectivity in the resting brain: a network analysis of the default mode hypothesis. Proc Natl Acad Sci U S A 2003;100:253–258

5. Raichle ME. What words are telling us about the brain. Cold Spring Harb Symp Quant Biol 1996;61:9–14

6. Raichle ME, MacLeod AM, Snyder AZ, Powers WJ, Gusnard DA, Shulman GL. A default mode of brain function. Proc Natl Acad Sci U S A 2001;98:676–682

7. Andrews-Hanna JR, Reidler JS, Sepulcre J, Poulin R, Buckner RL. Functional-anatomic fractionation of the brain's default network. Neuron 2010;65:550–562

8. Greicius MD, Srivastava G, Reiss AL, Menon V. Default-mode network activity distinguishes Alzheimer's disease from healthy aging: evidence from functional MRI. Proc Natl Acad Sci U S A 2004;101:4637–4642

9. Pfefferbaum A, Chanraud S, Pitel AL, et al. Cerebral blood flow in posterior cortical nodes of the default mode network decreases with task engagement but remains higher than in most brain regions. Cereb Cortex 2011;21:233–244

10. Vaishnavi SN, Vlassenko AG, Rundle MM, Snyder AZ, Mintun MA, Raichle ME. Regional aerobic glycolysis in the human brain. Proc Natl Acad Sci U S A 2010;107:17757–17762

11. Gusnard DA, Raichle ME, Raichle ME. Searching for a baseline: functional imaging and the resting human brain. Nat Rev Neurosci 2001;2:685–694

12. Minoshima S, Giordani B, Berent S, Frey KA, Foster NL, Kuhl DE. Metabolic reduction in the posterior cingulate cortex in very early Alzheimer's disease. Ann Neurol 1997;42:85–94

13. Hoogenboom WS, Marder TJ, Flores VL, et al. Cerebral white matter integrity and resting-state functional connectivity in middle-aged patients with type 2 diabetes. Diabetes 2014;63:728–738
14. Musen G, Jacobson AM, Bolo NR, et al. Resting-state brain functional connectivity is altered in type 2 diabetes. Diabetes 2012;61:2375–2379
15. Wolff SD, Balaban RS. Magnetization transfer contrast (MTC) and tissue water proton relaxation in vivo. Magn Reson Med 1989;10:135–144
16. van Waesberghe JH, Kamphorst W, De Groot CJ, et al. Axonal loss in multiple sclerosis lesions: magnetic resonance imaging insights into substrates of disability. Ann Neurol 1999;46:747–754
17. Schmierer K, Scaravilli F, Altmann DR, Barker GJ, Miller DH. Magnetization transfer ratio and myelin in postmortem multiple sclerosis brain. Ann Neurol 2004;56:407–415
18. Bruno SD, Barker GJ, Cercignani M, Symms M, Ron MA. A study of bipolar disorder using magnetization transfer imaging and voxel-based morphometry. Brain 2004;127:2433–2440
19. Hanyu H, Shimizu S, Tanaka Y, Kanetaka H, Iwamoto T, Abe K. Differences in magnetization transfer ratios of the hippocampus between dementia with Lewy bodies and Alzheimer's disease. Neurosci Lett 2005;380:166–169
20. Bagary MS, Symms MR, Barker GJ, Mutsatsa SH, Joyce EM, Ron MA. Gray and white matter brain abnormalities in first-episode schizophrenia inferred from magnetization transfer imaging. Arch Gen Psychiatry 2003;60:779–788
21. Association AD; American Diabetes Association. Standards of medical care in diabetes—2013. Diabetes Care 2013;36(Suppl .1):S11–S66
22. Fowler MJ. Microvascular and macrovascular complications of diabetes. Clin Diabetes 2008;26:77–82
23. Folstein MF, Folstein SE, McHugh PR. "Mini-mental state". A practical method for grading the cognitive state of patients for the clinician. J Psychiatr Res 1975;12:189–198
24. First MB, Spitzer RL, Gibbon M, Williams JB. *Structured Clinical Interview for Axis I DSM-IV Disorders*. New York, Biometrics Research, 1994
25. Hamilton M. Development of a rating scale for primary depressive illness. Br J Soc Clin Psychol 1967;6:278–296
26. Linn BS, Linn MW, Gurel L. Cumulative illness rating scale. J Am Geriatr Soc 1968;16:622–626
27. D'Agostino RB, Wolf PA, Belanger AJ, Kannel WB. Stroke risk profile: adjustment for antihypertensive medication. The Framingham Study. Stroke 1994; 25:40–43
28. Radloff LS. The CES-D scale: A self-report depression scale for research in the general population. Appl Psychol Meas 1977;1:385–401
29. Wechsler D. *Wechsler Test of Adult Reading: WTAR*. San Antonio, TX, Psychological Corporation, 2001
30. Steens SC, Bosma GP, Steup-Beekman GM, le Cessie S, Huizinga TW, van Buchem MA. Association between microscopic brain damage as indicated by magnetization transfer imaging and anticardiolipin antibodies in neuropsychiatric lupus. Arthritis Res Ther 2006;8:R38
31. Khaleeli Z, Altmann DR, Cercignani M, Ciccarelli O, Miller DH, Thompson AJ. Magnetization transfer ratio in gray matter: a potential surrogate marker for progression in early primary progressive multiple sclerosis. Arch Neurol 2008;65: 1454–1459
32. Audoin B, Davies G, Rashid W, Fisniku L, Thompson AJ, Miller DH. Voxel-based analysis of grey matter magnetization transfer ratio maps in early relapsing remitting multiple sclerosis. Mult Scler 2007;13:483–489
33. Chen JT, Collins DL, Atkins HL, Freedman MS, Arnold DL; Canadian MS/BMT Study Group. Magnetization transfer ratio evolution with demyelination and remyelination in multiple sclerosis lesions. Ann Neurol 2008;63:254–262
34. Bohner G, Milakara D, Witthaus H, et al. MTR abnormalities in subjects at ultra-high risk for schizophrenia and first-episode schizophrenic patients compared to healthy controls. Schizophr Res 2012;137:85–90
35. Bagley LJ, Grossman RI, Galetta SL, Sinson GP, Kotapka M, McGowan JC. Characterization of white matter lesions in multiple sclerosis and traumatic brain injury as revealed by magnetization transfer contour plots. AJNR Am J Neuroradiol 1999;20:977–981
36. Smith SA, Farrell JA, Jones CK, Reich DS, Calabresi PA, van Zijl PC. Pulsed magnetization transfer imaging with body coil transmission at 3 Tesla: feasibility and application. Magn Reson Med 2006;56:866–875
37. Smith SM, Fox PT, Miller KL, et al. Correspondence of the brain's functional architecture during activation and rest. Proc Natl Acad Sci U S A 2009;106: 13040–13045
38. Benjamini Y, Krieger AM, Yekutieli D. Adaptive linear step-up procedures that control the false discovery rate. Biometrika 2006;93:491–507
39. Benjamini Y, Hochberg Y. On the adaptive control of the false discovery rate in multiple testing with independent statistics. J Educ Behav Stat 2000;25: 60–83
40. Benjamini Y, Hochberg Y. Controlling the false discovery rate - a practical and powerful approach to multiple testing. J R Stat Soc B 1995;57:289–300
41. Manschot SM, Brands AM, van der Grond J, et al.; Utrecht Diabetic Encephalopathy Study Group. Brain magnetic resonance imaging correlates of impaired cognition in patients with type 2 diabetes. Diabetes 2006;55:1106–1113
42. Jongen C, van der Grond J, Kappelle LJ, Biessels GJ, Viergever MA, Pluim JP; Utrecht Diabetic Encephalopathy Study Group. Automated measurement of brain and white matter lesion volume in type 2 diabetes mellitus. Diabetologia 2007;50:1509–1516
43. Wu M, Rosano C, Butters M, et al. A fully automated method for quantifying and localizing white matter hyperintensities on MR images. Psychiatry Res 2006; 148:133–142
44. Leech R, Braga R, Sharp DJ. Echoes of the brain within the posterior cingulate cortex. J Neurosci 2012;32:215–222
45. Gilbert SJ, Dumontheil I, Simons JS, Frith CD, Burgess PW. Comment on "Wandering Minds: The Default Network and Stimulus-Independent Thought." Science 2007;317:43; author reply 43
46. Leech R, Kamourieh S, Beckmann CF, Sharp DJ. Fractionating the default mode network: distinct Contributions of the ventral and dorsal posterior cingulate cortex to cognitive control. J Neurosci 2011;31:3217–3224
47. Leech R, Sharp DJ. The role of the posterior cingulate cortex in cognition and disease. Brain 2014;137:12–32
48. Utevsky AV, Smith DV, Huettel SA. Precuneus is a functional core of the default-mode network. J Neurosci 2014;34:932–940
49. Reiman EM, Caselli RJ, Yun LS, et al. Preclinical evidence of Alzheimer's disease in persons homozygous for the epsilon 4 allele for apolipoprotein E. N Engl J Med 1996;334:752–758
50. Reiman EM, Chen K, Alexander GE, et al. Functional brain abnormalities in young adults at genetic risk for late-onset Alzheimer's dementia. Proc Natl Acad Sci U S A 2004;101:284–289